

http://pubs.acs.org/journal/aesccq Article

# Spectroscopic Investigation of the High-Pressure Behavior of Aliphatic Hydrocarbon: Implications for Planetary Processes

Abhisek Basu,\* Mainak Mookherjee, Christina Schiffert, Bianca Haberl, and Reinhard Boehler



**Cite This:** *ACS Earth Space Chem.* 2021, 5, 449–456



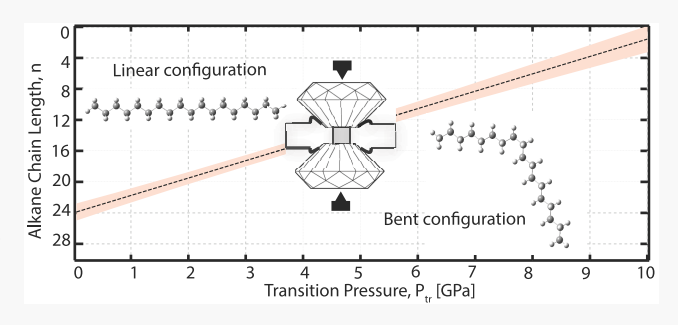
**ACCESS** 

III Metrics & More

Article Recommendations

s Supporting Information

ABSTRACT: Octadecane ( $C_{18}H_{38}$ ) is an aliphatic hydrocarbon that is abundant in carbonaceous chondritic meteorites. It is debated whether these hydrocarbons found in the meteorite are pristine or are a result of subsequent modifications as these meteorites are delivered to the Earth. It is well-known that meteorites are often subjected to extreme pressures and temperatures upon entering the Earth's atmosphere. To explore the behavior of octadecane at high pressures, that is, how its molecular structure responds to compression, we use a diamond anvil cell in conjunction with Raman spectroscopy. We find that at room temperatures, upon compression to  $\sim$ 5 GPa, a linear-chain



octadecane molecule transforms into a bent-chain configuration. Similar transitions from linear to a bent configuration in other hydrocarbons have been documented. We find a linear correlation between the transition pressure from linear to bent configuration, and the chain length of the alkane, that is, longer chain lengths, is likely to be less stable in the linear configuration under compression. These kinks in the bent-chain configuration are likely sites for the dissociation of the longer chain hydrocarbons to smaller hydrocarbons. The octadecane sample examined in this study did not undergo any additional transition to the highest pressure ( $\sim$ 18 GPa) explored in this study.

KEYWORDS: octadecane, carbonaceous chondritic meteorite, high pressures, Raman spectroscopy, diamond anvil cell

## ■ INTRODUCTION

Earth is a unique terrestrial planet and is the only one in our solar system known to harbor complex life. How and when did life begin on Earth, how did life evolve, and how were the ingredients for harboring life delivered are some of the fundamental questions pertaining to the understanding of the evolution of life on Earth. Fossil records of stromatolite and microfossils and carbon isotopic evidence of biological activity have been observed as early as 3500 Ma. 1-3 The origin of life in these early earth-forming episodes is often linked with the delivery of essential prebiotic organic matter via extra-terrestrial inputs including interplanetary dust particle (IDP), cometary, asteroidal, and meteorite impacts.<sup>4,5</sup> The size of the extraterrestrial matter might have been crucial in the delivery of these prebiotic organic matters, for instance, IDPs and meteorites that were small enough to gradually sink through the early Earth atmosphere may have avoided extensive modification upon entering the atmosphere. 5,6 Carbonaceous chondritic (CC) meteorites are considered to be undifferentiated representative of the most pristine matter resembling solar chemistry and are also known to contain several weight percent of organic material.7-10 Organic matter found in these carbonaceous chondrites is either free organic matter or macromolecular material.7 The CC meteorites are known to contain various types of organic compounds including amino acids, alcohols, aldehydes, aliphatic and aromatic hydrocarbons, ketones, and others. 7,11 The origin of aliphatic hydrocarbons in CC meteorites has been extensively explored but their origin is often debated. 7,11,12 The presence of abundant quantities of aliphatic hydrocarbon, that is, n-alkane, has been reported in several meteorites including Orgueil (CI1), Alais (CI1), Tonk (CI1), Ivuna (CI1), and Murray (CM2). 13-16 It was suggested that these n-alkanes observed in these meteorites may have originated in the condensing solar nebula through the Fischer-Tropsch mechanism.<sup>17</sup> Further analysis although showed that these *n*-alkanes were often concentrated on the surface hinting toward terrestrial contamination. 18-20 However, the extraterrestrial origin of aliphatic hydrocarbons has been supported by analysis of the Tagish Lake meteorite just after the impact, thereby avoiding terrestrial contamination, with n-alkanes present in major abundances and C<sub>23</sub> as the most abundant. <sup>11,21</sup> Furthermore, a recent study on the Paris meteorite<sup>22</sup> has revealed the presence of *n*-alkanes with the carbon chain length

Received: September 13, 2020 Revised: January 26, 2021 Accepted: January 27, 2021 Published: February 10, 2021





ranging between  $C_{16}$  and  $C_{25}$ , without the typical signature of terrestrial contamination. Among these n-alkanes,  $C_{17}$  (heptadecane) and  $C_{18}$  (octadecane) were the most abundant ones.

To address whether these *n*-alkanes are indigenous to these meteorites, we need to have a better understanding of whether these *n*-alkanes survive the pressure and temperature conditions that the meteorites experience as they enter the Earth's atmosphere and during the subsequent impacts. For instance, the smaller-sized IDPs and micrometeorites experience temperatures over 500 °C during atmospheric entry and passage.<sup>2</sup> It is speculated that extreme conditions experienced by the meteorites, comets, and IDPs may likely result in extensive modification of its original constituent organic matter. To better understand the high-pressure and high-temperature behavior of hydrocarbons, static and shock high-pressure high-temperature experiments have been conducted on hydrocarbons and they indicate indeed that these hydrocarbons undergo significant modifications<sup>8,10,27–35</sup> (Supporting Information Table ST1). Upon compression to ~2 GPa and at temperatures of ~1000-1500 K, methane (CH<sub>4</sub>) polymerizes to longer-chain alkanes and also forms graphite (C) and molecular hydrogen (H<sub>2</sub>).<sup>34</sup> The formation of unsaturated hydrocarbons is also reported at higher temperatures. <sup>28,29</sup> Upon compression up to 5 GPa and at temperatures of ~1500 K, ethane (C<sub>2</sub>H<sub>6</sub>) transforms into a mixture of relatively longer-chain hydrocarbons such as propane  $(C_3H_8)$ , butane  $(C_4H_{10})$ , and methane  $(CH_4)$  and carbon (C).<sup>34</sup> At pressure  $\sim$ 1 GPa, heptane (C<sub>7</sub>H<sub>16</sub>) undergoes a firstorder phase transition from liquid to solid state. 36,37 Extensive studies have been conducted to understand the behavior of nalkanes (up to  $C_{15}$ ) at high pressures and temperatures. However, the high-pressure and high-temperature behaviors of n-alkanes with  $C_{16}$ - $C_{25}$  remain relatively unknown and it will be crucial to test whether these large-chain hydrocarbons are indigenous to CC meteorites, are transformed products, or are terrestrial contamination. It will be important to understand whether subjecting meteorites to pressures and temperatures will lead to the dissociation of large-chain *n*-alkanes. If the largechain n-alkanes undergo dissociation, it will be important to understand the underlying mechanisms and the final products. In this study, we examine the pressure response of a saturated aliphatic hydrocarbon octadecane ( $C_{18}H_{38}$ ; n = 18, i.e.,  $C_{18}$ ) that is abundant in meteorites.22

## ■ METHOD

We have obtained the crystalline linear-chain octadecane sample from Alfa Aesar with >99% purity. Due to the low melting point (28 °C) of the sample, we followed a procedure during loading ensuring that it was not inadvertently exposed to temperatures above its melting point. We collected the ambient and highpressure Raman spectra of the octadecane sample using a Horiba Jobin Yvon LabRAM Evolution Raman spectrometer located at the Earth Materials Laboratory, Department of Earth, Ocean and Atmospheric Sciences, Florida State University. We used a 1800 l/mm grating which set the resolution of the spectrometer to 2 cm<sup>-1</sup>. We collected the Raman spectra using a frequencydoubled solid-state Nd-YAG laser with a 532 nm wavelength. To focus the laser within the diamond cell, we used a 50× infinitycorrected long working distance objective. We used symmetric cells for static compressions, that is, compression at room temperature. The symmetric cells were equipped with an ultralow fluorescence Type Ia diamond pair with a culet size of 300  $\mu$ m. We preindented the gasket to ~50  $\mu$ m thickness and a sample cavity was drilled at the center of the indented metal

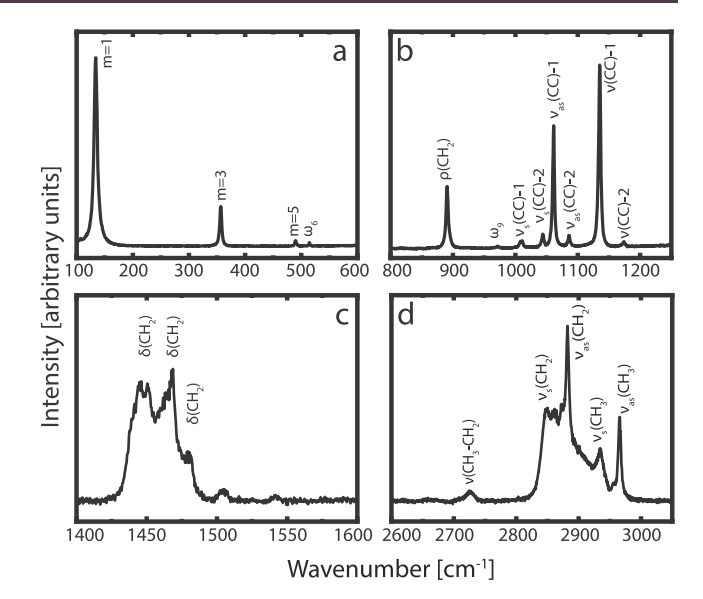
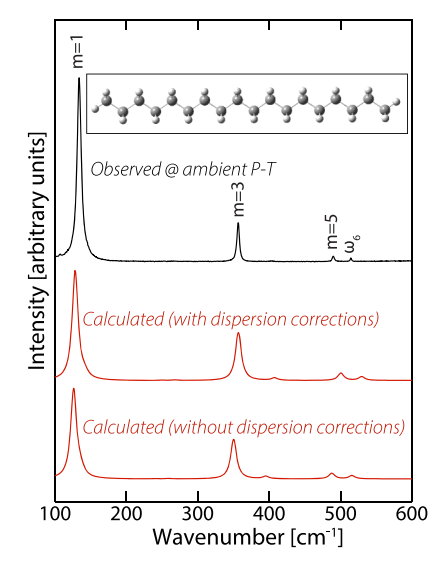


Figure 1. Raman spectrum of octadecane at ambient pressures and temperatures. (a) Low-energy region between 100 and 600 cm<sup>-1</sup> is characterized by the LAM and is indicated by m=1, 3, and 5. (b) Energy region between 800 and 1250 cm<sup>-1</sup> is characterized by symmetric and asymmetric C–C stretching modes ( $\nu$ ) and vibrations related to H–C–H rocking modes ( $\rho$ ). (c) Energy region between 1400 and 1600 cm<sup>-1</sup> is characterized by H–C–H bending or scissoring motions ( $\delta$ ). (d) High-energy region between 2600 and 3000 cm<sup>-1</sup> is characterized by vibrations due to symmetric and asymmetric C–H stretching modes ( $\nu$ ).



**Figure 2.** Raman spectrum in the low-energy region between 100 and 600 cm $^{-1}$ . The spectral pattern in black is the observed Raman spectrum of octadecane under ambient pressure and temperature conditions. The fundamental LAMs and the overtones are indicated by m=1, 3, and 5. The calculated spectra (in red) of the linear octadecane chain with the B3LYP/6-311++G\*\* method resulted in good wavenumber agreement with the observed values (Table 1). To account for the dispersion forces, the Grimme's D3 $^{42}$  corrections were added to the B3LYP/6-311++G\*\*. A molecular structure of linear octadecane is shown in the inset. The dark gray spheres represent carbon atoms and the light gray smaller spheres represent hydrogen atoms.

gasket using the electrospark erosion technique. We used a stainless-steel foil with a 150  $\mu m$  thickness for the static

compression. Due to the waxy nature of the sample, we loaded it without any pressure media. Few micron-size grains of ruby were also loaded as a pressure marker.<sup>38</sup>

To interpret the Raman spectra at high pressures, we have performed first-principles simulations on C<sub>18</sub>H<sub>38</sub> with different configurations. We have used the GAUSSIAN 09W<sup>39</sup> and optimized the geometry of the C<sub>18</sub>H<sub>38</sub> using the B3LYP<sup>40,41</sup> energy functionals. We have employed the 6-311++G\*\* basis set for the calculations. To account for the dispersive forces between the alkane chains, we have added Grimme's Dispersion D3 correction. 42 We have probed three types of chain configurations—linear, bent, and hairpin (Figures 2 and 4). The linear and bent octadecane structure was created using the GaussView software. In the bent configuration, we introduced the kink at half the length of the chain, that is, an equal number of carbons atoms on each segment of the chain (i, j = 9, Figure)4). In addition, we also explored an octadecane chain with a hairpin bend, as reported in earlier studies. 43 The longer part of the hairpin segment was composed of eight adjacent carbon atoms and the shorter part contained 2 adjacent carbon atoms (Figure 4). We used GaussSum<sup>44</sup> to determine the magnitude of the vibrational energy/frequency. The full-width at half maximum (fwhm) was fixed at 1 cm<sup>-1</sup>, and the intensities were scaled by a factor of 1.

### RESULTS

## Raman Spectra of Octadecane at Ambient Pressure.

The ambient condition Raman spectra of octadecane exhibit vibrations related to the (a) cooperative longitudinal motion of the carbon atoms in the hydrocarbon chain mimicking an accordion, that is, longitudinal accordion mode (LAM), (b) C—C stretching ( $\nu$ ) mode, (c) H—C—H twisting ( $\tau$ ) modes (d) H—C—H bending ( $\delta$ ) modes, and (e) C—H stretching ( $\nu$ ) modes (Figure 1). The low-energy region between 100 and 600 cm<sup>-1</sup> is dominated by LAMs. The fundamental LAM is a low-energy mode and observed at wavenumber <500 cm<sup>-1</sup>. In the case of octadecane, the fundamental LAM (m=1) is observed at 131 cm<sup>-1</sup>, and the overtones at 357 cm<sup>-1</sup> (m=3) and 490 cm<sup>-1</sup> (m=3) (Table 1). The LAMs of the hydrocarbon chains are inversely related to the size lengths of the chain and have been discussed

Table 1. Deconvoluted Raman Modes under Ambient Conditions from Experimental Measurements and Calculations

	f	frequency [cm		
		calcı	ılated	
Raman modes	observed	with dispersion	without dispersion	assignment
accordion modes	131	128	126	m = 1
	357	357	350	m = 3
	490	501	488	m = 5
$\omega_6$	514	530	516	
$\rho(\mathrm{CH_2})$	891	901	896	CH <sub>2</sub> rock
$\omega_9$	972			
$\nu_{\rm s}({ m CC})$ -1	1011	1019	1013	CC symmetric stretch
$\nu_{\rm s}({ m CC})$ -2	1044	1058	1049	CC symmetric stretch
$\nu_{\rm as}({ m CC})$ -1	1061	1068	1065	CC asymmetric stretch
$\nu_{\rm as}({ m CC})$ -2	1086	1102	1098	CC asymmetric stretch
ν(CC)-1	1135	1149	1147	CC stretch
$\nu$ (CC)-2	1174	1202	1202	CC stretch
$\delta(\mathrm{CH_2})$	1443	1492	1488	CH <sub>2</sub> bending
	1468	1495	1491	
	1480	1499	1499	
$\nu$ (CH <sub>3</sub> -CH <sub>2</sub> )	2726			CH <sub>3</sub> -CH <sub>2</sub> stretch
$\nu_{\rm s}({ m CH_2})$	2847	2995	2995	CH <sub>2</sub> symmetric stretch
$\omega_{13}$	2859			
$\omega_{14}$	2879			
$ u_{\rm as}({ m CH_2})$	2882	3006	3007	CH <sub>2</sub> asymmetric stretch
$\nu_{\rm s}({ m CH_3})$	2931	3015	3017	CH <sub>3</sub> symmetric stretch
$\nu_{\rm as}({ m CH_3})$	2966	3081	3081	CH <sub>3</sub> asymmetric stretch

extensively in an earlier report.<sup>32</sup> In addition to LAMs, a weak peak at 514 cm<sup>-1</sup> is also observed (Figure 1).

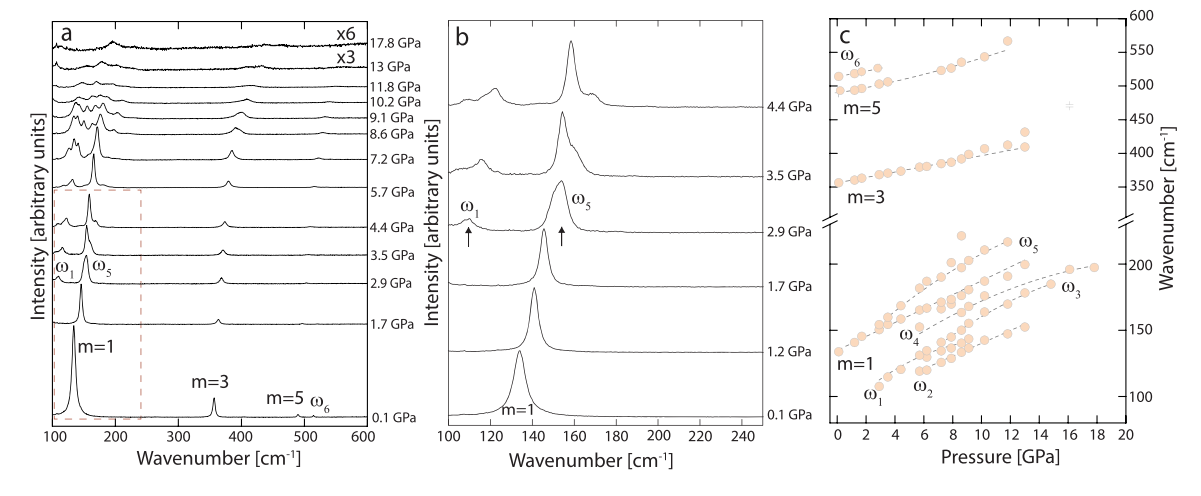


Figure 3. (a) Pressure evolution stack plot of selective Raman spectra of octadecane in the region  $100-600 \, \mathrm{cm}^{-1}$ . The accordion modes are marked with m values. The new modes,  $\omega_1-\omega_5$ , are observed at high pressure. The wavenumber region below  $100 \, \mathrm{cm}^{-1}$  was not considered for its proximity to the notch filter cutoff frequency. The high-pressure plots are scaled 3-6 times to highlight the modes. The spectra within the dashed box region are magnified in the plot (b). (b) Pressure evolution stack plot of Raman spectra of octadecane in the region  $100-250 \, \mathrm{cm}^{-1}$  upto 4.4 GPa. Arrows indicate the appearance of new modes at 2.9 GPa. (c) Plot shows the deconvoluted Raman mode frequency as a function of pressure. The dashed gray lines are polynomial fit to the measured data points (light orange filled circles).

Table 2. Pressure Dependence of Deconvoluted Modes

vibration	frequency [cm <sup>-1</sup> ]	$\partial  u/\partial P \ [\mathrm{cm}^{-1}/\mathrm{GPa}]$	remark
$\omega_1$	108	$10.1 \pm 4.0$	appears at 2.9
$\omega_2$	119	$4.8 \pm 0.3$	appears at 5.7
fundamental accordion mode, $m = 1$	134	$5.3 \pm 0.1$	
$\omega_3$	141	$11.8 \pm 3.5$	appears at 7.2
$\omega_4$	153	$8.7 \pm 3.6$	appears at 5.7
$\omega_5$	154	$10.5 \pm 1.2$	appears at 2.9
overtone accordion mode, $m = 3$	357	$4.1 \pm 0.1$	
overtone accordion mode, $m = 5$	490	$3.8 \pm 0.4$	
$\omega_6$	514	$4.0 \pm 0.2$	
CH <sub>2</sub> rock	891	$3.6 \pm 0.3$	
$\omega_7$	896	$0.6 \pm 0.1$	appears at 4.4
$\omega_8$	916	$3.6 \pm 0.1$	appears at 4.4
$\omega_9$	972	$4.6 \pm 0.5$	
CC symmetric stretch	1011	$5.6 \pm 0.2$	
CC symmetric stretch	1044	$4.6 \pm 0.1$	
CC asymmetric stretch	1061	$3.8 \pm 0.4$	
CC stretch	1086	$4.6 \pm 0.4$	
CC stretch	1135	$4.5 \pm 0.2$	
CC stretch	1174	$0.7 \pm 0.1$	
CH <sub>2</sub> twist	1296	$2.5 \pm 0.1$	
CH <sub>2</sub> bend	1443	$5.5 \pm 0.1$	
CH <sub>2</sub> bend	1468	$6.0 \pm 0.5$	
CH <sub>3</sub> -CH <sub>2</sub> stretch	2726	$6.3 \pm 0.2$	
CH <sub>2</sub> symmetric stretch	2847	$11.2 \pm 0.5$	
$\omega_{13}$	2859	$11.2 \pm 4.7$	
$\omega_{14}$	2879	$14.0 \pm 1.2$	
CH <sub>2</sub> asymmetric stretch	2882	$27.0 \pm 1.6$	
CH <sub>3</sub> symmetric stretch	2931	$13.3 \pm 0.5$	
CH <sub>3</sub> asymmetric stretch	2966	$13.5 \pm 0.2$	

The ambient Raman spectrum in the energy region between 800 and 1250 cm<sup>-1</sup> of octadecane is characterized by rocking motions of the H-C-H cluster of atoms with  $\rho(CH_2) \sim 891$ cm<sup>-1</sup>. This region is also characterized by symmetric stretching of C-C atom pairs with  $\nu_s$  (CC)-1 ~1011 cm<sup>-1</sup> and  $\nu_s$  (CC)-2~ 1044 cm<sup>-1</sup> and asymmetric stretching of C-C atom pairs with  $\nu_{\rm as}({\rm CC})$ -1: 1061 cm<sup>-1</sup> and  $\nu_{\rm as}({\rm CC})$ -2: 1086 cm<sup>-1</sup>. Two additional modes observed at 1135 and 1174 cm<sup>-1</sup> are also likely to be associated with the C-C stretching motion. The energy region between 1400 and 1600 cm<sup>-1</sup> is characterized by bending or scissoring vibrations of the H-C-H clusters. The high-energy region between 2600 and 3000 cm<sup>-1</sup> is characterized by C-H stretching vibrations (Table 1).

Static Pressure Dependence of Raman Modes of Octadecane. To understand the behavior of the Raman modes at high pressures, the octadecane was compressed at room temperature up to ~18 GPa in a symmetric diamond anvil cell. In the low-energy region between 100 and 600 cm<sup>-1</sup>, the modes observed under ambient conditions stiffened upon compression. We observed pressure-induced reduction of intensity for all the LAMs including the fundamental and overtones, that is, m = 1, 3, and 5. LAMs were not detectable

above ~14 GPa (Figure 3). In addition, upon compression, we observed several new modes including  $\omega_1 \sim 108 \text{ cm}^{-1}$  and  $\omega_5 \sim$ 154 cm<sup>-1</sup> at 2.9 GPa,  $\omega_2 \sim 119 \text{ cm}^{-1}$  and  $\omega_4 \sim 153 \text{ cm}^{-1}$  at 5.7 GPa, and  $\omega_3 \sim 141 \text{ cm}^{-1}$  at 7.2 GPa (Table 2, Figure 3, and Supporting Information Figure SF1). The pressure dependence of these pressure-induced new modes, that is,  $\partial \omega_i / \partial P$ , where i =1-5, ranges between 6.8 and 11.8 cm<sup>-1</sup>/GPa. The  $\partial \omega_i/\partial P$  of the pressure-induced new modes is significantly higher than the pressure dependence of the LAMs, that is,  $\partial m_i/\partial P$  where i=13, ranging from 3.8 to 5.3 cm<sup>-1</sup>/GPa. This indicates that these new modes are softer and likely related to vibration with a weaker force constant. To understand these pressure-induced low-energy (<200 cm<sup>-1</sup>) modes ( $\omega_i$ , where i = 1-5), we used first-principles simulations to calculate Raman spectra of an octadecane molecule with a bent and a hairpin configuration (Figure 4). Comparing the observed Raman spectra at 4.4 GPa and the calculated Raman spectra for the octadecane molecule with linear, bent, and hairpin configurations, it is likely that the pressure-induced modes are associated with the bent configurations (Figure 4). To accurately assign the spectral modes observed on compression, the pressure evolution of the crystal structure obtained from complementary studies such as neutron/X-ray scattering must be considered in the firstprinciples calculation, which requires further study.

On compression, the modes in the intermediate-energy region ~800-1250 cm<sup>-1</sup>, that is, C-C stretching modes,  $\nu(CC)$ , and vibrations related to H-C-H rocking modes,  $\rho(CH_2)$ , are observed to stiffen (Figure 5). Additionally, the modes in the intermediate-energy region  $\sim 1400-1600$  cm<sup>-1</sup>, that is, bending or scissoring vibrations of the H-C-H clusters,  $\delta(CH_2)$ , and the modes in the high-energy region ~2600–3200 cm<sup>-1</sup>, that is, C–H stretching vibrations,  $\nu$ (CH), stiffened upon compression (Figure 6). The rocking mode,  $\rho(CH_2) \sim 891$ cm<sup>-1</sup>, stiffens upon compression and remains intense up to the maximum pressures explored in this study. Upon an increase in pressure to 4.4 GPa, we observe the development of shoulder modes  $[\omega_7$  and  $\omega_8]$  on either side of the  $\rho(CH_2)$  mode. The weak shoulder modes could not be deconvoluted beyond ∼10 GPa. An extra mode  $[\omega_9]$  of the unknown origin at 972 cm<sup>-1</sup> also increases in frequency with pressure; however, it was not discernible at higher pressures and could not be deconvoluted beyond 4 GPa. The symmetric and asymmetric stretching frequencies for the C-C cluster of atoms in the wavenumber range from 1000 to 1250 cm<sup>-1</sup> increase with pressure and show significant broadening at high pressures. The pressure dependence of most of the C–C stretching modes (i.e.,  $\partial \nu / \partial P$ ) varies between 4 and 5.6 cm<sup>-1</sup>/GPa, except for the mode at 1174 cm<sup>-1</sup> [ $\nu$ (CC)-2] which remains fairly insensitive to pressure with  $\partial \nu$ /  $\partial P = 0.7 \text{ cm}^{-1}/\text{GPa}$  (Table 2) and disappears around 7 GPa, portraying a soft-mode-type behavior. 45,46 All the C-H<sub>2</sub> bending mode  $[\delta(CH_2)]$  frequencies increase with pressure and show severe broadening beyond 3 GPa. Consequently, above 3 GPa, only a broad mode was observed at the C-H<sub>2</sub> bending frequency region, as distinguishing individual modes were beyond the resolution of our spectrometer. In the C-H stretching region from wavenumber 2700-3000 cm<sup>-1</sup>, the modes were observed to stiffen and broaden with compression. The mode due to CH<sub>3</sub>-CH<sub>2</sub> stretching vibrations gradually decreased in intensity and could not be observed beyond 11.8 GPa (Figure 6). Except for the two modes ( $\omega_{13}$  and  $\omega_{14}$ ), likely due to CH stretching motions, the other symmetric and asymmetric CH stretching modes did not persist up to the highest pressure explored in this study.

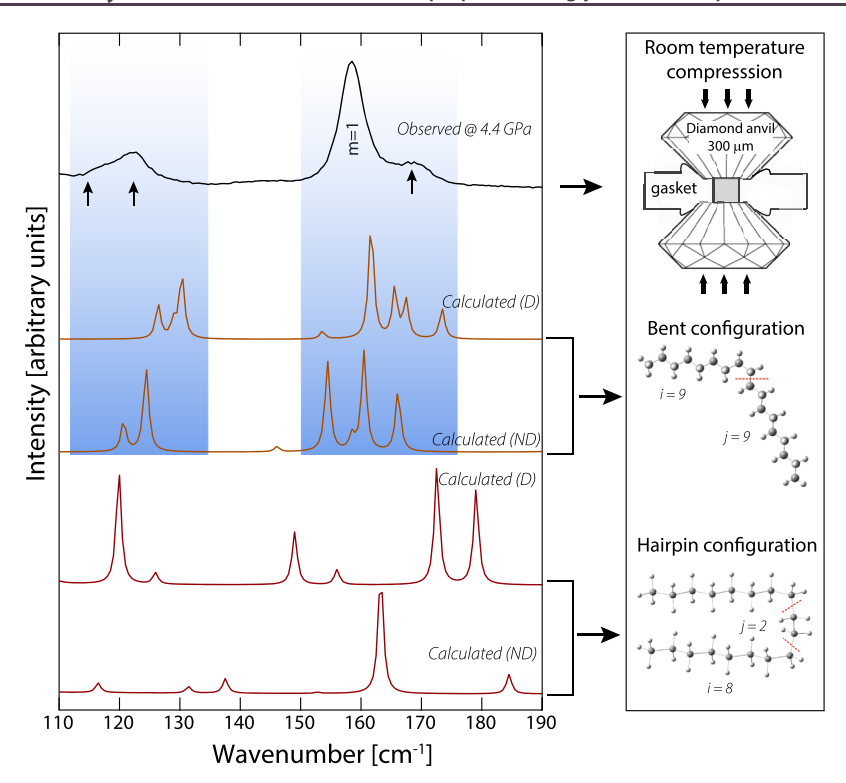


Figure 4. Observed and calculated Raman spectra in the low wavenumber region <200 cm<sup>-1</sup>. The observed spectrum in the wavenumber region of <200 cm<sup>-1</sup> at 4.4 GPa (represented in black) is characterized by the fundamental accordion mode, m = 1, and new modes at wavenumber <160 cm<sup>-1</sup> (indicated with arrows). The adjacent panel shows a schematic diamond anvil cell diagram employed in this experiment using 300  $\mu$ m diamond culets. The calculated spectra for the bent structure with and without dispersion are represented in orange color and the simulated bent structure is shown in the adjacent panel. The bent structure contained nine carbon atoms (i, j = 9) on each segment of the chain. The observed and the calculated modes for the bent structure show a good agreement in the low wavenumber region (blue shaded area). The calculated Raman spectra for the hairpin structure with and without dispersion are represented in red color and the simulated hairpin structure is shown in the adjacent panel. The longest segment of the hairpin has eight adjacent carbon atoms (i = 8) and the shortest segment has two atoms (i = 2) [D = with dispersion; ND = no dispersion].

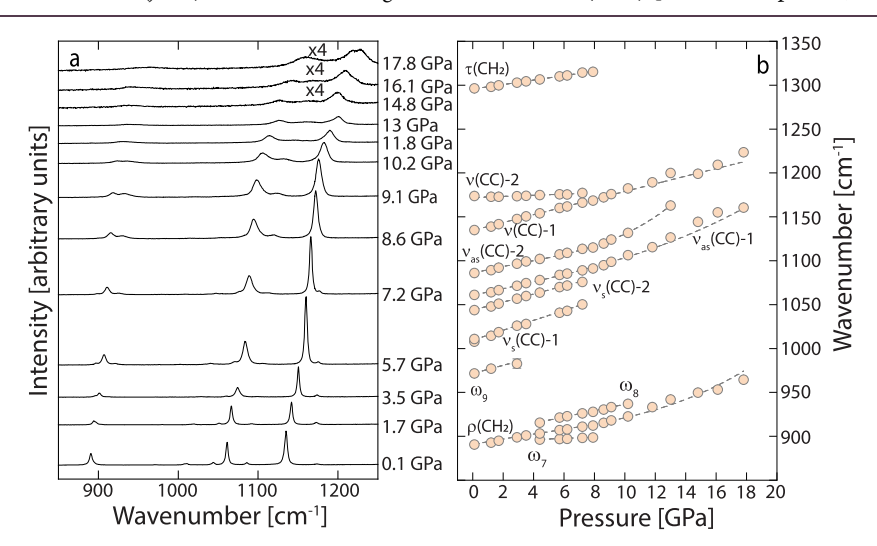


Figure 5. (a) Pressure evolution stack plot of selective Raman spectra of octadecane in the region 850–1250 cm<sup>-1</sup>. (b) Plot shows the deconvoluted Raman mode frequency as a function of pressure. The dashed gray lines are polynomial fit to the measured data points (light orange filled circles).

## DISCUSSION

In general, the linear-chain alkanes are energetically favored over bent/hairpin structures up to a critical chain length,  $n_{\rm c}=16-17.^{43,47-49}$  Beyond this critical chain length, the attractive intramolecular forces will aid in the formation of a hairpin/folded state from the linear chain in the absence of another perturbative field. In this study, experimental observations and complimentary *first-principles* simulations indicate that upon

compression, the molecular structure of octadecane ( $C_{18}H_{38}$ ) evolves from a linear to a bent-chain configuration around  $\sim 3$  GPa. At high pressures, although, a transition to a hairpin/folded state appears unlikely based on a comparison between the observed and calculated spectra (Figure 4). Our results on octadecane are similar to a recent study on tricosane ( $C_{23}H_{48}$ ), which also reveal pressure-induced new low wavenumber modes, albeit at a lower pressure of 0.3 GPa. The appearance

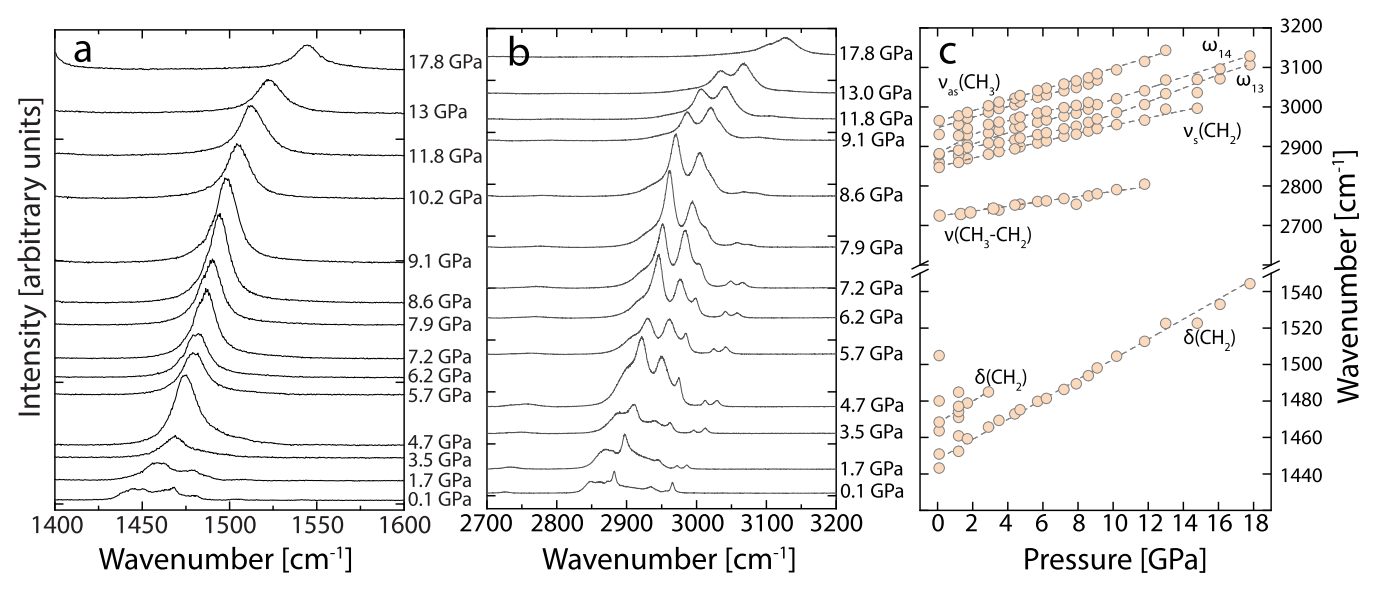
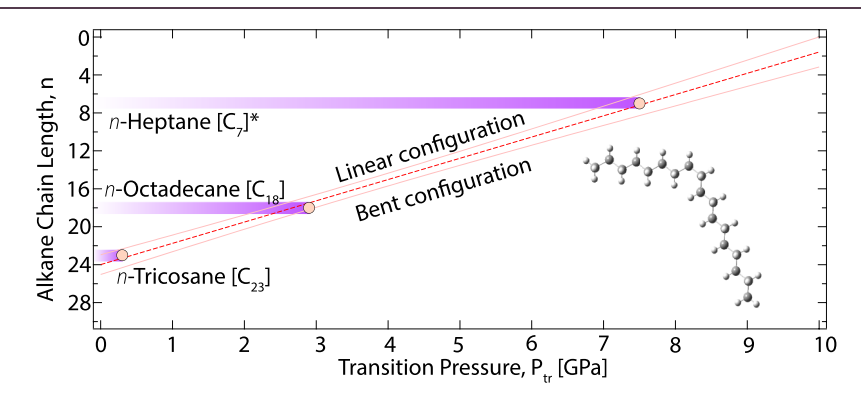


Figure 6. (a) Pressure evolution stack plot of selective Raman spectra of octadecane in the region  $1400-1600~{\rm cm}^{-1}$ . The region shows CH<sub>2</sub> bending ( $\delta$ ) modes for the octadecane. (b) Pressure evolution stack plot of selective Raman spectra of octadecane in the region  $2700-3200~{\rm cm}^{-1}$ . The region shows the CH<sub>n</sub> cluster of atom stretching modes ( $\nu$ ). (c) Plot shows the deconvoluted Raman mode frequency as a function of pressure. The dashed gray lines are polynomial fit to the measured data points (light orange filled circles).



**Figure 7.** Plot represents the pressure-induced bending of linear-chain alkanes—tricosane, octadecane, and heptane (\*).<sup>37</sup> Increasing chain length results in the lowering of the linear—bend transition pressure. A bent octadecane chain configuration is shown in the inset.

of the new modes was attributed to bent-chain configurations.<sup>32</sup> Similar transformations have been also observed in *n*-heptane which undergoes a solid-solid all trans-conformer transition and associated pressure-induced changes in the low wavenumber external modes above 7.5 GPa.<sup>37</sup> We suspect that the gauche-trans transition is accompanied by a bending of the nheptane chain above 7.5 GPa. We find a linear correlation between the chain length and the transition pressures between linear and bent configuration. It is expected that the energy requirement for bending a chain will decrease with the increasing number of the carbon atom. Our correlations indicate that for a chain length  $> C_{24}$ , the chain is likely to bend at moderate to ambient pressures (Figure 7). However, we recognize that this correlation is based on a limited number of chain lengths examined and a systematic study on *n*-alkane with different chain lengths is warranted for evaluating this proposition.

The formation of the bent structure at high pressures has implications on the dissociation mechanism of alkanes. Long-chain alkanes ( $C_{18}$  and  $C_{19}$ ) are known to undergo complete dissociation at high pressure and temperature into nano-diamonds;<sup>33</sup> however, the exact dissociation mechanisms are not well understood. The probable mechanism of dissociation

will likely depend on the actual P-T path followed.<sup>32</sup> While this present study cannot confirm the dissociation of long-chain alkanes, it certainly provides valuable insights into the breakdown mechanism. Our observations demonstrate that static compression leads to the bending of the linear chains. The kinks in the bent structure are likely to act as the nucleus that is likely to facilitate the eventual dissociation of the larger chains at relevant temperatures, that is, aided by sufficient thermal energy.

The octadecane reveals remarkable phase stability over the pressure range discussed in this study. Aside from the appearance of the low wavenumber modes around 4–5 GPa, no other distinct changes in the spectral pattern were observed that would be indicative of a transformation/dissociation to a different compound. Similar phase stability as a function of pressure was observed for tricosane to 23 GPa. The phase stability of  $C_{18}$  and  $C_{23}$  over a large range of pressure indicates that the aliphatic hydrocarbons, likely, would have survived the impact experienced by the interplanetary dust particles or microsized meteorites during the exogenous delivery of organic matter in the late heavy bombardment period (4.5–3.8 Ga). The absence of any dissociation/polymerization with compression of large-chain aliphatic hydrocarbon implies that the pressure range explored in this study will not transform n-

alkanes to organic precursor complex molecules, which are essential for life.

#### ASSOCIATED CONTENT

## **Solution** Supporting Information

The Supporting Information is available free of charge at https://pubs.acs.org/doi/10.1021/acsearthspace-chem.0c00259.

Selective summary of experiments on aliphatic hydrocarbons (n-alkanes) at high pressures and temperatures; comparison between observed and calculated mode frequencies; and deconvoluted Raman spectra of octadecane at 1.7 GPa, 2.9 GPa, and 3.5 GPa (PDF)

## AUTHOR INFORMATION

#### **Corresponding Author**

Abhisek Basu — Earth Materials Laboratory, Department of Earth, Ocean and Atmospheric Science, Florida State University, Tallahassee, Florida 32306, United States;
orcid.org/0000-0002-0283-1778; Email: abasu@fsu.edu

#### **Authors**

Mainak Mookherjee — Earth Materials Laboratory, Department of Earth, Ocean and Atmospheric Science, Florida State University, Tallahassee, Florida 32306, United States; orcid.org/0000-0002-0605-5964

Christina Schiffert – Earth Materials Laboratory, Department of Earth, Ocean and Atmospheric Science, Florida State University, Tallahassee, Florida 32306, United States

Bianca Haberl — Neutron Scattering Division, Neutron Sciences Directorate, Oak Ridge National Laboratory, Oak Ridge, Tennessee 37831, United States; orcid.org/0000-0002-7391-6031

Reinhard Boehler – Neutron Scattering Division, Neutron Sciences Directorate, Oak Ridge National Laboratory, Oak Ridge, Tennessee 37831, United States

Complete contact information is available at: https://pubs.acs.org/10.1021/acsearthspacechem.0c00259

#### Notes

The authors declare no competing financial interest. Notice of Copyright: This manuscript has been authored by UT-Battelle, LLC under contract no. DE-AC05-00OR22725 with the U.S. Department of Energy. The United States Government retains and the publisher, by accepting the article for publication, acknowledges that the United States Government retains a nonexclusive, paid-up, irrevocable, world-wide license to publish or reproduce the published form of this manuscript or allow others to do so, for United States Government purposes. The Department of Energy will provide public access to these results of federally sponsored research in accordance with the DOE Public Access Plan (http://energy.gov/downloads/doe-public-access-plan).

## ■ ACKNOWLEDGMENTS

This work is funded by the National Science Foundation (NSF) (EAR 1753125, 1638752, and 1248553). A.B. acknowledges the Dean's Teaching Postdoctoral Fellowship from the College of Arts and Sciences, Florida State University. A.B. and C.S. acknowledge the Undergraduate Research Opportunity Program, Florida State University. B.H. and R.B. were supported by resources at the Spallation Neutron Source and the High Flux

Isotope Reactor, DOE Office of Science User Facilities operated by the Oak Ridge National Laboratory (ORNL). Authors acknowledge the computing resources from the High Performance Computing, Research Computing Center, Florida State University.

#### REFERENCES

- (1) Bennett, J.; Donahue, M.; Schneider, N.; Voit, M. *The Essential Cosmic Perspective*, 6th ed.; Pearson Education: San Francisco, 2012.
- (2) Schopf, J. W.; Kudryavtsev, A. B.; Czaja, A. D.; Tripathi, A. B. Evidence of Archean Life: Stromatolites and Microfossils. *Precambrian Res.* **2007**, *158*, 141–155.
- (3) Schopf, J. W. Fossil Evidence of Archaean Life. *Philos. Trans. R. Soc.*, B **2006**, 361, 869–885.
- (4) Chyba, C.; Thomas, P.; Brookshaw, L.; Sagan, C. Cometary Delivery of Organic Molecules to the Early Earth. *Science* **1990**, 249, 366–373.
- (5) Chyba, C.; Sagan, C. Endogenous Production, Exogenous Delivery and Impact-Shock Synthesis of Organic Molecules: An Inventory for the Origins of Life. *Nature* **1992**, *355*, 125–132.
- (6) Anders, E. Pre-Biotic Organic Matter from Comets and Asteroids. *Nature* **1989**, 342, 255–257.
- (7) Sephton, M. A. Organic Compounds in Carbonaceous Meteorites. *Natural Product Reports*; The Royal Society of Chemistry May 23, 2002; Vol. 19, pp 292–311.
- (8) Potiszil, C.; Montgomery, W.; Sephton, M. A. Effects of Pressure on Model Compounds of Meteorite Organic Matter. *ACS Earth Space Chem.* **2017**, *1*, 475–482.
- (9) Botta, O.; Bada, J. L. Extraterrestrial Organic Compounds in Meteorites. *Surv. Geophys.* **2002**, 23, 411–467.
- (10) Jennings, E.; Montgomery, W.; Lerch, P. Stability of Coronene at High Temperature and Pressure. *J. Phys. Chem. B* **2010**, *114*, 15753–15758.
- (11) Pizzarello, S.; Cooper, G. W.; Flynn, G. J. The Nature and Distribution of the Organic Material in Carbonaceous Chondrites and Interplanetary Dust Particles. In *Meteorites and the Early Solar System II*; Lauretta, D. S., McSween, H. Y., Jr, Eds.; University of Arizona Press: Tucson, 2006; pp 625–651.
- (12) Glavin, D. P.; Alexander, C. M. O.; Aponte, J. C.; Dworkin, J. P.; Elsila, J. E.; Yabuta, H. The Origin and Evolution of Organic Matter in Carbonaceous Chondrites and Links to Their Parent Bodies. In *Primitive Meteorites and Asteroids*; Elsevier, 2018; pp 205–271.
- (13) Nagy, B.; Meinschein, W. G.; Hennessy, D. J. Mass Spectroscopic Analysis of the Orgueil Meteorite: Evidence for Biogenic Hydrocarbons. *Ann. N.Y. Acad. Sci.* **2006**, *93*, 27–35.
- (14) Meinschein, W. G. Benzene Extracts of the Orgueil Meteorite. *Nature* **1963**, 197, 833–836.
- (15) Meinschein, W. Hydrocarbons in Terrestrial Samples and the Orgueil Meteorite. *Space Sci. Rev.* **1963**, *2*, 653–679.
- (16) Meinschein, W. G.; Nagy, B.; Hennessy, D. J. Evidence in Meteorites of Former Life: The Organic Compounds in Carbonaceous Chondrites Are Similar to Those Found in Marine Sediments. *Ann. N.Y. Acad. Sci.* **2006**, *108*, 553–579.
- (17) Studier, M. H.; Hayatsu, R.; Anders, E. Origin of organic matter in early solar system-I. Hydrocarbons. *Geochim. Cosmochim. Acta* **1968**, 32, 151–173.
- (18) Nooner, D. W.; Oró, J. Organic compounds in meteorites-I. Aliphatic hydrocarbons. *Geochim. Cosmochim. Acta* **1967**, 31, 1359–1394.
- (19) Oró, J.; Nooner, D. W. Aliphatic Hydrocarbons in Meteorites. *Nature* **1967**, *213*, 1085–1087.
- (20) Han, J.; Simoneit, B. R.; Burlingame, A. L.; Calvin, M. Organic Analysis on the Pueblito de Allende Meteorite. *Nature* **1969**, 222, 364–365.
- (21) Pizzarello, S.; Cooper, G. W. Molecular and Chiral Analyses of Some Protein Amino Acid Derivatives in the Murchison and Murray Meteorites. *Meteorit. Planet. Sci.* **2001**, *36*, 897–909.

- (22) Martins, Z.; Modica, P.; Zanda, B.; d'Hendecourt, L. L. S. The Amino Acid and Hydrocarbon Contents of the Paris Meteorite: Insights into the Most Primitive CM Chondrite. *Meteorit. Planet. Sci.* **2015**, *50*, 926–943.
- (23) Flynn, G. J. Atmospheric Entry Heating: A Criterion to Distinguish between Asteroidal and Cometary Sources of Interplanetary Dust. *Icarus* 1989, 77, 287–310.
- (24) Love, S.; Brownlee, D. E. Heating and Thermal Transformation of Micrometeoroids Entering the Earth's Atmosphere. *Icarus* **1991**, *89*, 26–43.
- (25) Brownlee, D. E.; Joswiak, D. J.; Love, S. G.; Bradley, J. P. Identification of Cometary and Asteroidal Particles in Stratospheric Idp Collections. In 24th Lunar and Planetary Science Conference; 1993; pp 205–206.
- (26) Sandford, S. A.; Bradley, J. P. Interplanetary Dust Particles Collected in the Stratosphere: Observations of Atmospheric Heating and Constraints on Their Interrelationship and Sources. *Icarus* 1989, 82, 146–166
- (27) Puerto, M. A.; Balzaretti, N. M. Raman and Infrared Vibrational Modes of Tricosane Paraffin under High Pressure. *Vib. Spectrosc.* **2014**, 75, 93–100.
- (28) Lobanov, S. S.; Chen, P.-N.; Chen, X.-J.; Zha, C.-S.; Litasov, K. D.; Mao, H.-K.; Goncharov, A. F. Carbon Precipitation from Heavy Hydrocarbon Fluid in Deep Planetary Interiors. *Nat. Commun.* **2013**, *4*, 2446.
- (29) Benedetti, L. R.; Nguyen, J. H.; Caldwell, W. A.; Liu, H.; Kruger, M.; Jeanloz, R. Dissociation of CH4 at High Pressures and Temperatures: Diamond Formation in Giant Planet Interiors? *Science* 1999, 286, 100–102.
- (30) Kraus, D.; Vorberger, J.; Pak, A.; Hartley, N. J.; Fletcher, L. B.; Frydrych, S.; Galtier, E.; Gamboa, E. J.; Gericke, D. O.; Glenzer, S. H.; Granados, E.; MacDonald, M. J.; MacKinnon, A. J.; McBride, E. E.; Nam, I.; Neumayer, P.; Roth, M.; Saunders, A. M.; Schuster, A. K.; Sun, P.; van Driel, T.; Döppner, T.; Falcone, R. W. Formation of Diamonds in Laser-Compressed Hydrocarbons at Planetary Interior Conditions. *Nat. Astron.* **2017**, *1*, 606–611.
- (31) Kraus, D.; Hartley, N. J.; Frydrych, S.; Schuster, A. K.; Rohatsch, K.; Rödel, M.; Cowan, T. E.; Brown, S.; Cunningham, E.; van Driel, T.; Fletcher, L. B.; Galtier, E.; Gamboa, E. J.; Laso Garcia, A.; Gericke, D. O.; Granados, E.; Heimann, P. A.; Lee, H. J.; MacDonald, M. J.; MacKinnon, A. J.; McBride, E. E.; Nam, I.; Neumayer, P.; Pak, A.; Pelka, A.; Prencipe, I.; Ravasio, A.; Redmer, R.; Saunders, A. M.; Schölmerich, M.; Schörner, M.; Sun, P.; Turner, S. J.; Zettl, A.; Falcone, R. W.; Glenzer, S. H.; Döppner, T.; Vorberger, J. High-Pressure Chemistry of Hydrocarbons Relevant to Planetary Interiors and Inertial Confinement Fusion. *Phys. Plasmas* **2018**, *25*, 056313.
- (32) Basu, A.; Murphy, P.; Mookherjee, M.; Haberl, B.; Boehler, R. High-Pressure Behavior of a Linear Chain Alkane, Tricosane. *J. Appl. Phys.* **2020**, *127*, 105901.
- (33) Zerr, A.; Serghiou, G.; Boehler, R.; Ross, M. Decomposition of Alkanes at High Pressures and Temperatures. *High Pressure Res.* **2006**, 26, 23–32.
- (34) Kolesnikov, A.; Kutcherov, V. G.; Goncharov, A. F. Methane-Derived Hydrocarbons Produced under Upper-Mantle Conditions. *Nat. Geosci.* **2009**, *2*, 566–570.
- (35) Kolesnikov, A. Y.; Saul, J. M.; Kutcherov, V. G. Chemistry of Hydrocarbons Under Extreme Thermobaric Conditions. *ChemistrySelect* **2017**, *2*, 1336–1352.
- (36) Krishnan, M.; Balasubramanian, S. n-Heptane under Pressure: Structure and Dynamics from Molecular Simulations. *J. Phys. Chem. B* **2005**, *109*, 1936–1946.
- (37) Kavitha, G.; Narayana, C. Raman Scattering Studies onn-Heptane under High Pressure. J. Phys. Chem. B 2006, 110, 8777–8781.
- (38) Mao, H. K.; Bell, P. M.; Shaner, J. W.; Steinberg, D. J. Specific volume measurements of Cu, Mo, Pd, and Ag and calibration of the rubyR1fluorescence pressure gauge from 0.06 to 1 Mbar. *J. Appl. Phys.* 1978, 49, 3276–3283.
- (39) Frisch, M. J.; Trucks, G. W.; Schlegel, H. B.; Scuseria, G. E.; Robb, M. A.; Cheeseman, J. R.; Scalmani, G.; Barone, V.; Petersson, G.

- A.; Nakatsuji, H.; Li, X.; Caricato, M.; Marenich, A. V.; Bloino, J.; Janesko, B. G.; Gomperts, R.; Mennucci, B.; Hratch, D. J. *Gaussian 09*; Gaussian, Inc.: Wallingford CT, 2009 Available at https://gaussian.com/glossary/g09/.
- (40) Becke, A. D. Density-functional thermochemistry. III. The role of exact exchange. *J. Chem. Phys.* **1993**, *98*, 5648–5652.
- (41) Lee, C.; Yang, W.; Parr, R. G. Development of the Colle-Salvetti Correlation-Energy Formula into a Functional of the Electron Density. *Phys. Rev. B: Condens. Matter Mater. Phys.* **1988**, *37*, 785–789.
- (42) Grimme, S.; Antony, J.; Ehrlich, S.; Krieg, H. A Consistent and Accurate Ab Initio Parametrization of Density Functional Dispersion Correction (DFT-D) for the 94 Elements H-Pu. *J. Chem. Phys.* **2010**, 132, 154104.
- (43) Byrd, J. N.; Bartlett, R. J.; Montgomery, J. A. At What Chain Length Do Unbranched Alkanes Prefer Folded Conformations? *J. Phys. Chem. A* **2014**, *118*, 1706–1712.
- (44) O'boyle, N. M.; Tenderholt, A. L.; Langner, K. M. Cclib: A Library for Package-Independent Computational Chemistry Algorithms. *J. Comput. Chem.* **2008**, *29*, 839–845.
- (45) Basu, A.; Chandra, A.; Tyagi, A. K.; Mukherjee, G. D. Reappearance of ferroelectric soft modes in the paraelectric phase of Pb1-xCaxTiO3at high pressures: Raman and x-ray diffraction studies. *J. Phys. Condens. Matter* **2012**, *24*, 115404.
- (46) Basu, A.; Jana, R.; Ranjan, R.; Mukherjee, G. D. Pressure effects on model ferroelectricBiFeO3–PbTiO3: Multiple phase transitions. *Phys. Rev. B* **2016**, *93*, 214114.
- (47) Lüttschwager, N. O. B.; Wassermann, T. N.; Mata, R. A.; Suhm, M. A. The Last Globally Stable Extended Alkane. *Angew. Chem., Int. Ed.* **2013**, *52*, 463–466.
- (48) Liakos, D. G.; Neese, F. Domain Based Pair Natural Orbital Coupled Cluster Studies on Linear and Folded Alkane Chains. *J. Chem. Theory Comput.* **2015**, *11*, 2137–2143.
- (49) Goodman, J. M. What Is the Longest Unbranched Alkane with a Linear Global Minimum Conformation? *J. Chem. Inf. Comput. Sci.* 1997, 37, 876–878.